J. Fluid Mech. (1986), *vol.* 169, *pp.* 513–533
Printed in Great Britain

Secondary vortices in the wake of circular cylinders

By T. WEI AND C. R. SMITH
Department of Mechanical Engineering and Mechanics, Lehigh University, Bethlehem, PA 18015, USA

(Received 13 September 1983 and in revised form 7 December 1985)

Using both the hydrogen-bubble flow-visualization technique and hot-wire-anemometry measurements, secondary vortices have been detected in the near-wake of circular cylinders and their characteristics studied over a Reynolds-number range of 1200–11000. The vortex-shedding characteristics of these secondary vortices clearly indicate that 'transition waves', detected in the cylinder near wake by Bloor (1964), and secondary vortices are identical phenomena. It is established that the non-dimensional shedding frequency of the secondary vortices demonstrates a 0.87 power-law relationship relative to Reynolds number, contrary to the 0.5 power-law reported by Bloor. The results suggest that the vortices result from a near-wake, free-shear instability which causes the separated cylinder boundary layer to roll up into the secondary vortices. Visual observations indicate that immediately following their formation the vortices undergo a strong three-dimensional distortion, which may provide the mechanism for the transition from laminar to turbulent Strouhal vortices.

1. Introduction

1.1. *Historical perspective*

Periodic shedding of vortices from circular cylinders has been studied for over a century. However, it is only recently that small-scale structures have been observed in the near-wake region. The apparent similarity between the structures observed in cylinder wake flows and free-shear flows suggests the existence of a universal transition mechanism from laminar to turbulent flows.

The first intensive dye-visualization study of three-dimensional structures in the near wake of cylinders at low Reynolds numbers was done by Gerrard (1978), who reported what he termed as 'knots' and 'fingers' regularly appearing in the flow. The 'knots' appeared as small kinks in the nominally two-dimensional Strouhal vortices. The 'fingers' were long streamwise filaments of dye which appeared to connect adjacent Strouhal vortices of like rotation. He was not able to describe what caused the 'knots' and 'fingers' and therefore did not pursue the matter.

Apparently similar structures have been observed in the near wake of free-shear mixing layers. Briedenthal (1979) used chemically reacting fluids to visually observe spanwise waviness in a shear layer. Observations made by Konrad (1976) and Bernal (1981) using shadowgraph techniques revealed long, streamwise 'braid' structures. Konrad speculated that the 'braids' were hairpin-type vortices created by a Taylor instability in the shear layer. He further speculated that these vortices contribute to the mass and momentum transfer between the high- and low-speed flows; he concluded that these transfer phenomena are mechanisms for the onset of turbulence in free-shear mixing layers. Bernal (1981), using a detailed frame-by-frame motion

picture analysis, developed a model of a secondary flow structure riding on the perimeter of large-scale mixing-layer vortices. His model illustrates a strong spanwise deformation and the streamwise stretching of vorticity concentrations between successive mixing-layer vortices, yielding a sinuous pattern of contiguous hairpin-type vortices 'riding' on and around the essentially two-dimensional mixing-layer vortices.

An important work on the transition to turbulence of cylinder wake flows was published by Bloor (1964). Employing hot-wire anemometers in air, Bloor observed an instability phenomenon in the near wakes of both a 0.635 cm and a 2.54 cm diameter cylinder. The phenomenon, termed 'transition waves' by Bloor, was apparently unrelated to the Strouhal vortex-shedding process. Bloor's results suggested that a square-root power-law relation exists between the non-dimensional transition-wave frequency and Reynolds number. She speculated that the transition waves were Tollmein–Schlichting waves in the separated boundary layer, and that these waves somehow contributed to the transition from vortex streets to turbulence. She did not speculate how this process takes place.

Wei & Smith (1980) used hydrogen bubbles in conjunction with a high-speed video recording system to observe 'axial vortex pairs' in the near wake of a 1.27 cm diameter cylinder over a Reynolds-number range of 100–3000. It was theorized that these vortices were stretched by the vortex street to form the 'fingers' reported by Gerrard (1978). Further, it was suggested that these vortex pairs were significant contributors to the transition from laminar to turbulent vortex streets.

1.2. *Hypothesis of secondary vortices in the cylinder near wake*

As pointed out in the previous section, observations of three-dimensional, secondary structures are quite common in free-shear mixing layers (Konrad 1976; Briedenthal 1979; Bernal 1981). The term 'secondary' is used throughout this paper to imply a phenomenon which is separate and distinctly different in appearance from the main, large-scale, periodic structures in the flow. This is not meant to imply that the secondary vortices differ in origin from the Strouhal vortices, since they both form from the same separated shear layer. A suggestion for the origin of these secondary structures (see Ho & Huerre 1984) is that they develop initially as two-dimensional instabilities as described by Michalke (1965). They then amplify to a level where they become three-dimensionally unstable. Further temporal amplification then yields three-dimensional vortices which create the 'braids' perceived in the studies cited above.

It seems reasonable that a similar evolution might occur in the near wake of a circular cylinder. If secondary vortices develop in a cylinder near wake, they should arise either in the unstable shear layer formed by the boundary layer separating from the cylinder, or in the cylinder boundary layer just prior to separation, where the velocity profile has already developed an inflexion point. Intuitively, it seems unlikely that the latter possibility would be the correct one; the boundary layer is extremely thin (even at separation), and the favourable pressure gradient on the leading portion of the cylinder, essentially up to the separation point, would tend to delay or damp the amplification of any instabilities. Thus the most logical suggestion for the origin of secondary vortices is that they develop in the boundary layer separating from the cylinder.

To examine this hypothesis, it is assumed that the shear layer can be approximated as a parallel mixing layer subject to the linear stability results of Michalke (1965). Michalke solved the Helmholtz equations for a perturbed free-shear layer with a

hyperbolic tangent velocity profile. He determined that the frequency at which the shear layer oscillates should scale on the ratio of the free-stream velocity to the momentum thickness θ of the layer. Although application of Michalke's analysis to the separated cylinder boundary layer may appear to be a crude approximation, it has been shown by Michalke & Hermann (1982), for a jet flow, that when d/θ is large, the amplification factors for the jet are essentially identical with those predicted by a linear stability analysis of a single parallel mixing layer. For the conditions investigated in the cylinder-flow study presented in the present paper, d/θ was found to be large up to at least one cylinder diameter downstream of the separation point; it would thus appear that linear stability analysis should be applicable in the region very close to the cylinder.

As pointed out by Michalke (1969), parallel shear layers are initially most susceptible to two-dimensional instabilities. It has been demonstrated in a number of studies (see the review paper by Ho & Huerre 1984) that the most-amplified wave in a mixing layer corresponds to

$$\frac{f\theta}{U} \approx 0.032, \tag{1}$$

where f is the frequency, U is the average velocity across the mixing layer, and θ is the characteristic momentum thickness of the layer. Ho & Huerre further note that the constant in (1) holds to within $\pm 5\%$ for a wide variety of mixing layers. Unal & Rockwell (1986) determined that the streamwise growth rate of the momentum thickness of a separated cylinder boundary layer, $\mathrm{d}\theta/\mathrm{d}x$, is approximately 0.04. The above information, when used with values characteristic of the investigation presented in this paper, indicates that secondary instabilities should begin to amplify in the separated boundary layer at around $x/d \approx 0.2$. Thus, it appears that two-dimensional secondary vortices can occur, and that they should first appear as a result of free-shear instabilities in the separated boundary layer. This result is supported by the probe measurements of Bloor (1964), as will be discussed later.

As the separated boundary layer grows, and the two-dimensional instabilities amplify, a two-dimensional concentration of vorticity will develop and begin to evolve into a mature vortex. However, during this evolution the vorticity concentrations become subject to three-dimensional instabilities of a type suggested by Lin (1981). Lin found that the vortex layers between large-scale transverse vortex structures are three-dimensionally unstable to the strain field induced by the transverse structures. His results indicate that for a range of spanwise-periodic initial conditions, amplification and deformation of the vortex layers will result in formation of counter-rotating, streamwise vortices between the large transverse structures. These results are consistent with a numerical study done by Cain, Reynolds & Ferzinger (1981), and experimental observations of Bernal (1981) and Lasheras, Cho & Maxworthy (1986).

It is hypothesized that a similar type of three-dimensional evolution will occur for the case of secondary vortices developing in the cylinder near wake. In addition to Lin's (1981) work, Browand (1965) and Hama (1963) suggest that the secondary vortices are three-dimensionally unstable, and should deform in a spanwise wavy fashion. The salient difference between the evolution of secondary vortices in a cylinder wake and those occurring in plane-shear flows is the rate at which the three-dimensional deformation occurs; the secondary vortices in a cylinder wake should first appear between the boundary-layer separation point and the region of initial Strouhal-vortex formation and should deform much more rapidly. The rationale for the rapidity of the secondary-vortex evolution and deformation is the

presence of a 'heavy' forcing effect of the Strouhal vortex on the region of initial disturbance growth, as suggested by Unal & Rockwell (1986). This suggestion is a logical extension of the observations of Freymouth (1966) and Ho & Nosseir (1981) on the effects of weak low-frequency forcing on the formation of higher-frequency instabilities.

1.3. *Research objectives*

The present study reports on a secondary-vortex phenomenon which has been observed immediately downstream of the cylinder boundary-layer separation point using hydrogen-bubble flow visualization. These vortices appear to be initially aligned with the cylinder axis of symmetry. However, they quickly deform into a cellular pattern. It is speculated that these secondary vortices deform to create the axial vortex pairs reported by Wei & Smith (1980).

It is also believed that the secondary vortices are the same phenomenon as Bloor's transition waves. Both phenomena are generated immediately downstream of the boundary-layer separation point, and seem to have similar shedding characteristics. Thus, one motivation for this investigation was to determine if the two phenomena are identical.

Overall, the research objectives of this investigation are: to examine the characteristics of the secondary vortices generated in the near wake of circular cylinders; and to correlate both flow-visualization observations and hot-wire measurements of the secondary vortices with those made by Bloor.

2. Apparatus and experimental methods

The apparatus employed in this investigation consisted of a free-surface water channel, a set of right circular cylinders, a hydrogen-bubble-wire flow-visualization system, hot-wire-anemometry equipment, and a high-speed video recording system. The test section of the free-surface water channel was made of Plexiglas, measuring 0.86×0.30 m in cross-section and 5.0 m in length. The maximum flow rate in the channel was 1500 gallons per min. Details of the water channel can be found in Smith & Metzler (1983).

2.1. *Cylinders*

Four right circular cylinders were used in this investigation. The cylinders were 86 cm long with outer diameters of 2.54 cm, 3.81 cm, 4.83 cm and 5.84 cm. The smallest three cylinders were sections of Plexiglas tubing; the largest cylinder was a section of polyvinyl chloride (PVC) tubing. Each cylinder was smooth to the touch and rigidly clamped in the channel using the support illustrated in figure 1. Alignment of the cylinder (i.e. ensuring that the cylinder axis was perpendicular to the flow direction) was generally done by eye with satisfactory results.

2.2. *Visualization system*

An INSTAR high-speed video system, built by the Video Logic Corporation, was used to view and record the hydrogen-bubble-visualized flow. Utilizing synchronized strobe lights, the system frames at a rate of 120 frames per s with an effective shutter speed of 1/10000 s. The system's unique advantage of variable slow-motion playback, still framing, and slow-motion reverse playback allowed detailed analysis of the complexities of the real-time vortex interactions.

Hydrogen bubbles were generated using a 20 cm long, 0.025 mm diameter platinum wire. The bubble generator could produce up to 0.5 A of current at frequencies from

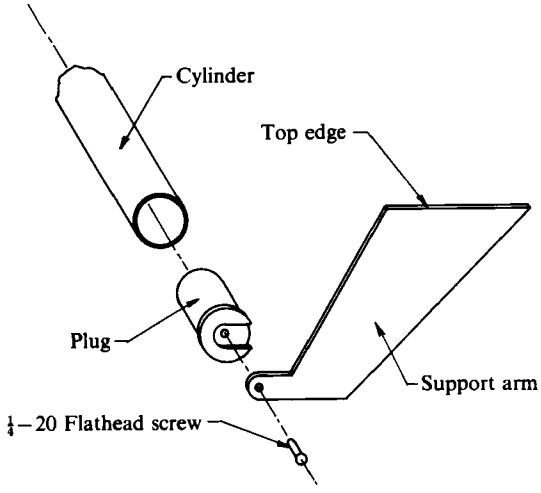

FIGURE 1. Schematic diagram of the cylinder support configuration for the largest three cylinders.

0 to 340 Hz, with the duration of the generated pulses variable from zero to infinity. Additional information about the hydrogen-bubble-wire flow-visualization system and the INSTAR video system are provided by Smith & Metzler (1983).

2.3. *Anemometry equipment*

The hot-wire anemometry equipment included a DISA type 55D01 constant-temperature anemometer, a DISA type 55R11 probe, a Krohn–Hite model 3700 band-pass filter, and a Digital Equipment Corporation (DEC) MINC-11 minicomputer. The minicomputer was equipped with an LS1 11/03 microprocessor and a 12-bit mantissa, DEC MNCAD, analog-to-digital converter.

2.4. *Visual data-acquisition techniques*

Data acquisition for the secondary-vortex investigation entailed collecting shedding-frequency information for a variety of flow conditions, and recording of video-tape sequences of hydrogen-bubble-visualized flow. Over forty combinations of free-stream velocity and cylinder diameter were examined. The method of data collection will be discussed below.

For each set of conditions, the channel centreline velocity and the water temperature were established, and a side-view video-tape sequence was taken. The shedding frequencies of the Strouhal vortices f_v and the secondary vortices f_i were then determind by reviewing the video tape. Top-view video sequencies were also recorded for selected sets of conditions.

Figures 2 and 3 are schematics showing the experimental configurations for the side-view and top-view visualization sequences. The origin of the coordinate system was centred on the cylinder axis of symmetry with all measurements taken at the spanwise centre of the channel, $z/L = 0$. The x-coordinate is defined as positive for locations downstream of the cylinder; the y-coordinate is positive for locations above the cylinder.

The shedding frequency of the Strouhal vortices was determined by ensemble-averaging five measurements of the time required for fifty vortices of like rotation to pass across the video picture. Similarly, the shedding frequency of the secondary

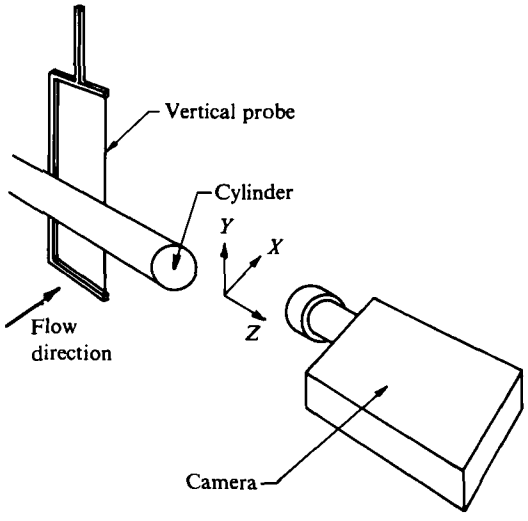

FIGURE 2. Oblique-view schematic showing the relative placement of the vertical bubble wire, the cylinder and the video camera. Coordinate system is centred on the cylinder axis of symmetry at the centre of the channel.

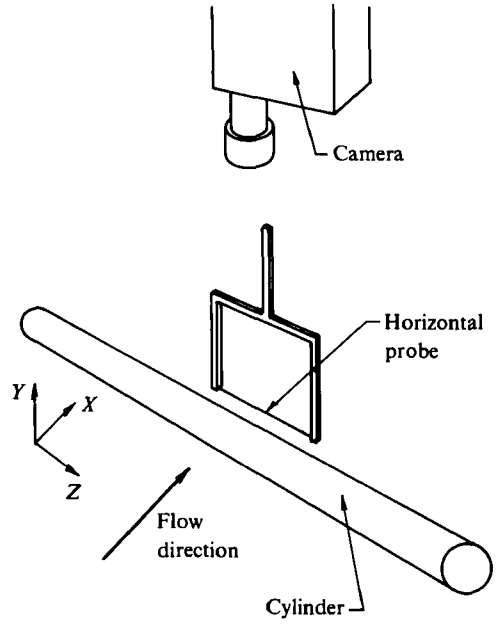

FIGURE 3. Oblique-view schematic showing the relative placement of the horizontal bubble wire, the cylinder and the video camera. Coordinate system is centred on the cylinder axis of symmetry at the centre of the channel.

vortices was obtained by averaging five determinations of the time required for the separated boundary layer to oscillate one hundred times. Because of the oscillatory and cellular (i.e. Lagrangian) nature of this phenomenon, this process was the most reproducible means of determining the secondary-vortex shedding frequency.

To examine the three-dimensional deformation of the secondary vortices, top-view video sequences were recorded for a number of conditions using the hydrogen-

bubble-wire configuration shown in figure 3. The wire was positioned consistently at the relative location $x/d = 0.5$ and $y/d = 0.5$. The video sequences were taken with the trailing edge of the cylinder aligned with the top of the picture, and the flow from top to bottom. It was these top-view studies which clearly revealed the spanwise cellular structure created by the three-dimensional deformation of the secondary vortices. Representative sequences from the video-tape studies are shown in conjunction with the results in §3.1.

3. Results and discussions

Flow over each cylinder was examined over a free-stream velocity range of 0.05 m/s–0.18 m/s, spanning an overall Reynolds-number range of approximately 1200–11000. The results of these studies are presented below.

3.1. *Photographic results*

In this section, photographic segments of top- and side-view video sequences are presented to illustrate the secondary-vortex development. The photographs were taken from recorded video sequences with the video monitor in stop-action mode.

Figure 4 is a set of photographs from a side-view video sequence which shows the secondary vortices as they appear at a Reynolds number of 2900. The flow was visualized with a vertical bubble wire which extended well above and below the cylinder. The non-dimensional time lapse, $\Delta t U_\infty/d$, between consecutive photographs is 0.49, equivalent to 10 % of the Strouhal-vortex shedding period. Schematics of the photographs are included to highlight the salient features of each photograph.

As shown in figure 4, the secondary vortices form in the shear layer between the free stream and the formation region, hereafter referred to as the separated boundary layer. The vortices are carried downstream by the Strouhal vortices, the flow field looking not unlike a ferris wheel of secondary vortices riding on the perimeter of a Strouhal vortex. The schematic diagrams accompanying the photographs illustrate this interaction. Each secondary vortex has been given an identification label. The letters t and b denote whether the secondary vortex was generated from the top or bottom of the cylinder, and the numbers signify the order in which the vortices were shed.

At this point, a comment is needed on the appropriateness of applying the term 'secondary', as defined in §1.2, to these vortices. The exact mechanism for the generation of Strouhal vortices is not well understood, making it difficult to satisfy the 'separate and distinct' criterion in the definition. The rationale for calling these smaller-scale vortices 'secondary vortices' is the degree of complexity of the two phenomena. As established in §1.2, the so-called 'secondary vortices' are hypothesized to be the result of the amplification of a free-shear instability in the separated boundary layer immediately downstream of the separation point. However, the generation of Strouhal vortices involves not only the vorticity in the separated boundary layer, but also the effect of the fluctuating base pressure in the vicinity of the rear stagnation point (see, for example, the paper by Bearman 1965). It is this interdependence between free-shear instability and pressure fluctuation which distinguishes the origin of the Strouhal vortex from the 'simpler' origin of the secondary vortices.

The above discussion does not discount the fact that the vorticity which amalgamates to form the Strouhal vortices must evolve in part from the secondary vortices,

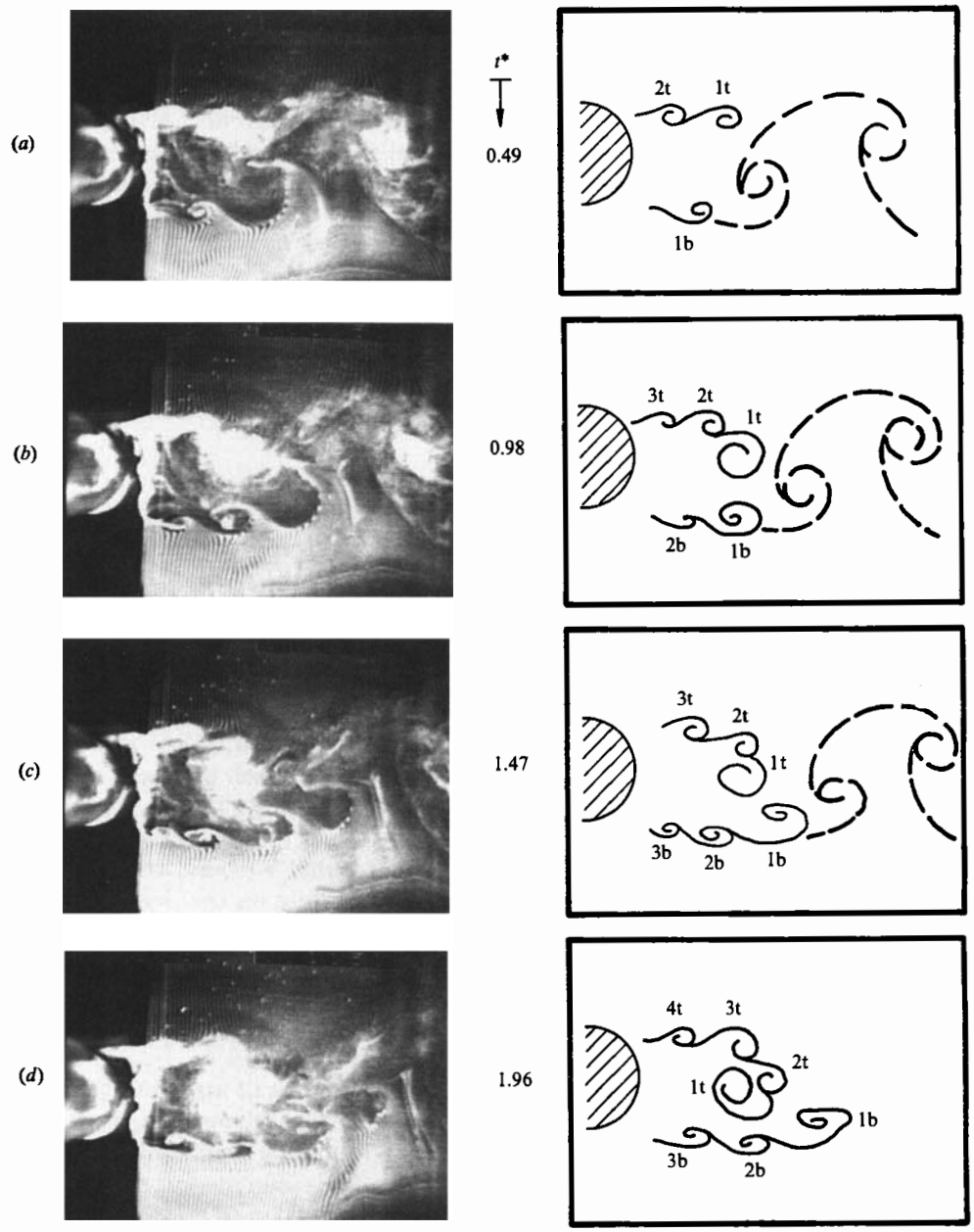

FIGURE 4. Side-view photographic sequence with schematics showing secondary vortices shed from the 4.83 cm cylinder at $Re_d = 2900$. The numbers indicate the order of shedding from the (t) top or (b) bottom of the cylinder. $t^* = \Delta t U_\infty / d$.

since both the secondary vortices and the Strouhal vortices derive their initial vorticity from the same separated shear layer. The process of this redistribution of vorticity is unclear. Initial appearances may suggest that the secondary vortices 'coalesce' into the Strouhal vortices, with the aid of the induced fluctuating base pressure. However, not all of the secondary vortices amalgamate into the Strouhal vortices; a portion appear to migrate into the shear layer between opposite-rotation

Strouhal vortices, where they undergo strong three-dimensional distortion due to the particularly strong strain field in that region. This latter process is similar to that shown by Ho & Huang (1982) to occur with weak forcing of a shear layer. An alternative description of the process of interaction is that the secondary and Strouhal vortices are instabilities of different wavelengths which evolve somewhat independently from the same shear layer, but via different processes. A similar type of observation for multiple-structure development in a plane shear layer is noted by Lasheras *et al.* (1986) for the development of secondary streamwise vortices superposed on primary spanwise vortices of the shear layer. Which of these processes is the correct interpretation of the observed behaviour is unclear, and cannot be answered from the results of the present study.

Figure 5 is a photographic sequence of top-view video-tape segments showing the three-dimensional nature of the secondary vortices. The Reynolds number is 2400 based on a cylinder diameter of 3.81 cm. The flow is top to bottom, with the trailing edge of the cylinder roughly aligned with the top of the pictures. The non-dimensional time lapse between successive photographs is 0.64 (i.e. 13 % of the Strouhal-vortex-shedding period). Schematic drawings of the secondary vortices, shown as solid lines, have been included to aid in interpreting the pictures. The sense of vorticity is indicated by arrows.

The vertical streaks of hydrogen bubbles in figure 5(*a*) illustrate the cellular nature of the secondary vortices and also serve as evidence of the streamwise stretching of the vortices. At the top of the figure a new secondary vortex is forming. Note that there appears to be a feedback mechanism between old and new vortices, evidenced by the alignment of new cells essentially directly behind older ones.

The roll-up of a Strouhal vortex can be deduced by observing the forward progress of the secondary vortices in figures 5(*c*, *d*). At the leading and trailing edges of a developing Strouhal vortex the streamwise velocity component approaches zero, whereas the streamwise velocity component is negative on the underside of the vortex. Thus when viewed from above a secondary vortex interacting with the forming Strouhal vortex appears to pause, reverse direction, and coalesce with other secondary vortices. The three-dimensional deformation of the secondary vortices thus accounts for the irregular shape of the Strouhal vortex in figure 5(*a*).

An idealization of the process of spanwise development of secondary vortices is shown schematically in figure 6 (a series of three top views), illustrating the deformation of a single, initially two-dimensional, secondary vortex. The direction of flow is top to bottom, with the sense of vorticity indicated by arrows. The time lapse between figure 6(*a*, *c*) is less than one-quarter of a Strouhal period.

Recall that in §1.2 it was hypothesized that the secondary vortices result from the amplification and roll-up of a two-dimensional instability in the separated boundary layer. This is represented by the straight line in figure 6(*a*). As the secondary vortex grows, it becomes increasingly susceptible to three-dimensional instabilities (figures 6*b*, *c*) as described by Hama (1963) and Lin (1981). It is clear from figure 6(*c*) that the three-dimensional deformation of secondary vortices will introduce streamwise vorticity to the flow field.

However, unlike the secondary vortices formed in plane-shear flows, it is hypothesized that the three-dimensional deformation is radically accelerated in the case of circular-cylinder flows. The additional source of streamwise stretching comes from the strong strain field generated by the Strouhal vortices, as illustrated in figure 7, which is an oblique-view schematic illustrating the manner in which a three-dimensional, secondary vortex interacts with Strouhal vortices of like rotation. The

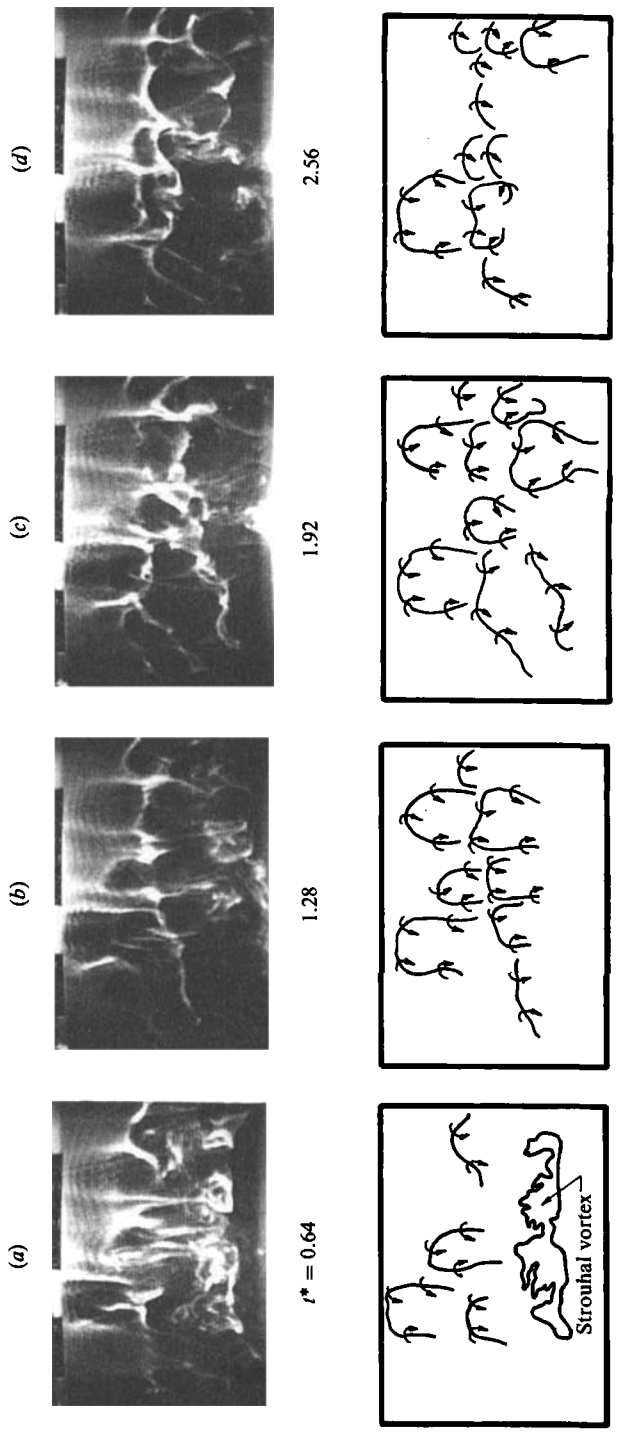

FIGURE 5. Top-view photographic sequence with schematics showing the cellular deformation of the secondary vortices shed from the 3.81 cm cylinder at $Re_d = 2400$. $t^* = \Delta t U_\infty / d$.

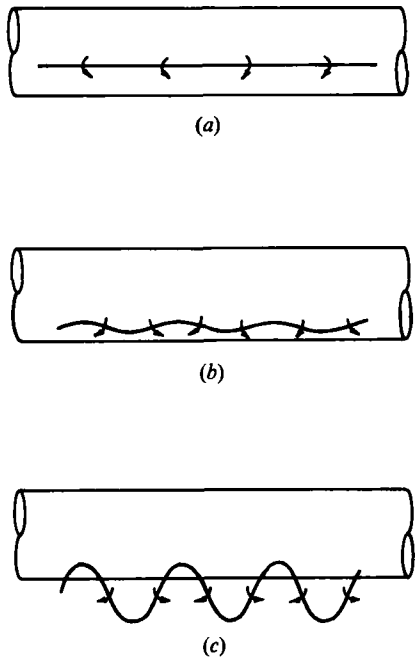

FIGURE 6. Top-view schematic sequence illustrating the growth of spanwise waviness in secondary vortices. An initially straight secondary vortex (*a*) deforms under three-dimensional perturbations (*b*), and becomes more wavy by self-induction (*c*). Flow is top to bottom.

flow is left to right with the Strouhal vortex depicted as a sheet, and the secondary vortex indicated by a line superimposed on the Strouhal vortex.

In reality, these are extreme idealizations, particularly since the Strouhal vortex may behave as a collective amalgamation of the secondary vortices, but the basic process suggested remains the same. The rotation of the Strouhal vortex shown in figure 7 primarily influences the leading segments of the deformed secondary vortex. Because the local velocity of the Strouhal vortex is higher than the velocity at the separation point, the leading segments of the secondary vortex will move faster than the trailing segments. This accentuates the amplitude of the spanwise waviness, and results in the stretching of streamwise vorticity.

More importantly, this stretching, which is essentially similar to the plane-shear case, is strongly augmented by the contribution of the Strouhal vortex of opposite rotation (not shown) which will be below and upstream of the vortex shown in figure 7. The effect of the counter-rotating Strouhal vortex is to pull the trailing segments of the secondary vortex down and upstream. Note that this occurs in the vicinity of initial secondary-disturbance growth and would generate the heavy forcing effect of the Strouhal vortices alluded to in §1.2. This strong added source of three-dimensional stretching, occurring so near the point of secondary-vortex formation, accounts for the rapid development of secondary vortices, and for the fact that they appear between the boundary-layer separation point and the Strouhal-vortex formation region. Note that a markedly similar interpretation and model are suggested by Lasheras *et al.* (1986) for stretching of secondary vortices by primary Kelvin–Helmholtz vortices in a developing free-shear layer.

A second top-view photographic sequence is shown in figure 8. This figures shows the 3.81 cm cylinder immersed in a flow with Reynolds number equal to 4530. The

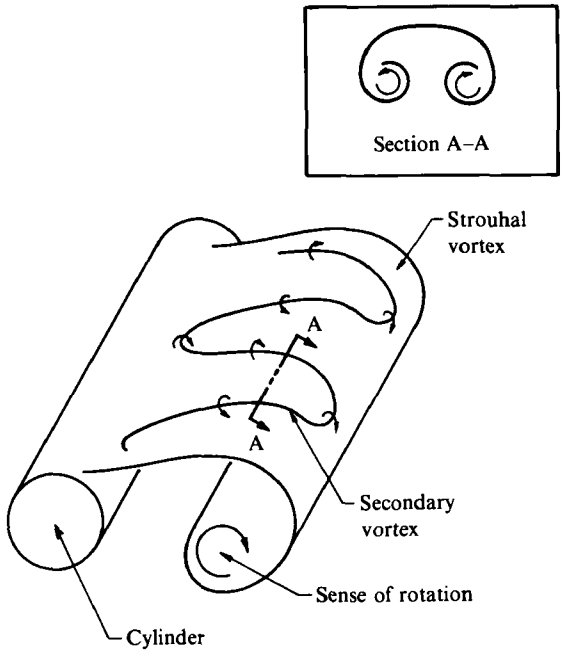

FIGURE 7. Oblique view illustrating the interaction between a secondary vortex and a Strouhal vortex. Section A–A shows the appearance of a streamwise vortex pair.

non-dimensional time lapse between successive photographs is 1.21, or 25% of a Strouhal period. The salient feature of this figure is that the secondary-vortex cells are smaller and more irregular than those in figure 5.

A final top-view sequence appears in figure 9 for a cylinder diameter of 4.83 cm and Reynolds number of 3570. The non-dimensional time lapse between successive photographs is 0.59, equivalent to 12% of the Strouhal period. In this sequence, the cellular structure of the secondary vortices appears less developed than for the smaller-diameter sequences. In fact, no secondary-vortex cell is readily apparent until the third frame, figure 9(*c*). In figure 9(*a*) the remnants of a secondary-vortex cell stretch across the left two-thirds of the photograph. While the streamwise alignment of subsequent cells can be seen to develop in figures 9(*b*, *c*), a well-developed cell does not appear until figure 9(*d*).

The alignment of vortex cells is evident in figure 9(*d*), supporting the hypothesis of a feedback mechanism. Also, note that the spanwise nature of the secondary vortices shown in figures 5, 8 and 9 appears consistent with the spanwise behaviour observed in the mixing-layer results of Konrad (1976). He observed that the average spanwise spacing of the secondary 'braid' between mixing-layer vortices scales on the order of the momentum thickness, with the spacing increasing with downstream distance as the momentum thickness grows. The initial momentum thickness of the separated boundary layer will be roughly equal to the momentum thickness of the boundary layer prior to separation. From Schlichting (1979), this value can be approximated as $d\,Re_d^{-\frac{1}{2}}$. Thus, at comparable Reynolds numbers the initial separated-boundary-layer thickness will increase with increasing diameter, yielding larger, wider-spaced cells. Likewise, an increase in Reynolds number for a fixed diameter will decrease the initial separated-boundary-layer thickness, which should

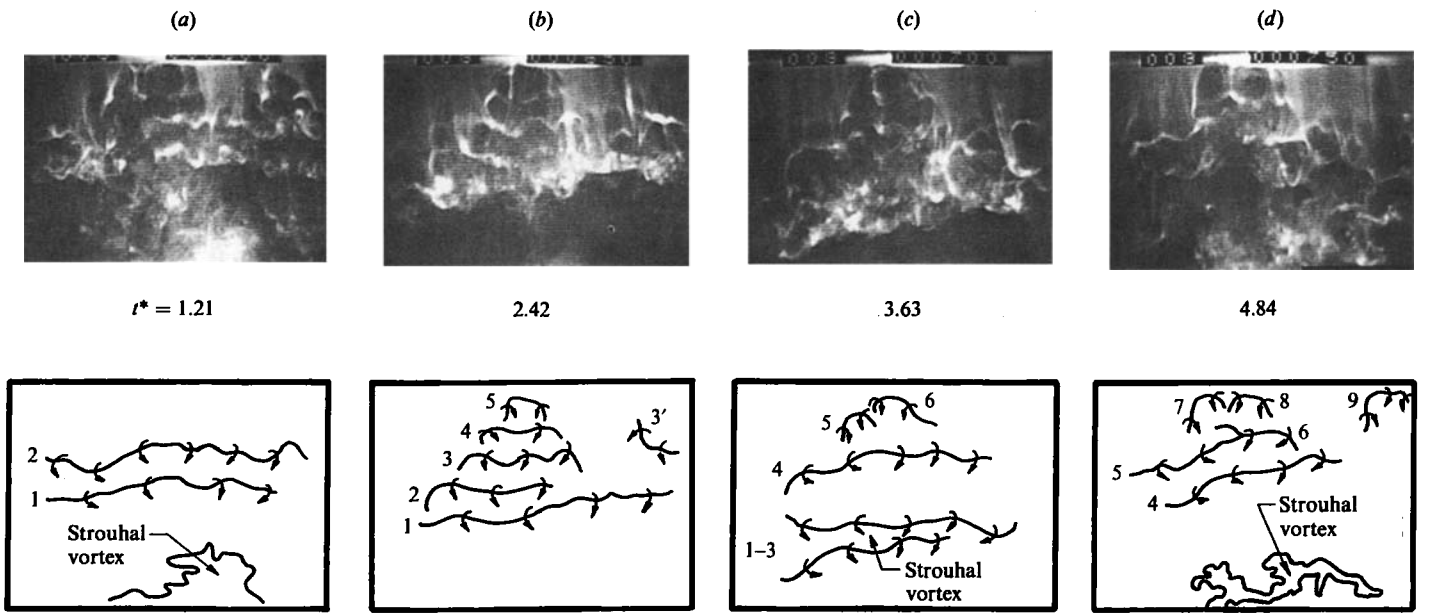

FIGURE 8. Top-view sequence showing the cellular deformation of the secondary vortices shed from a 3.81 cm cylinder at $Re_d = 4530$. $t^* = \Delta t U_\infty / d$. Note that the cells are less organized (i.e. more turbulent) than those in figure 5.

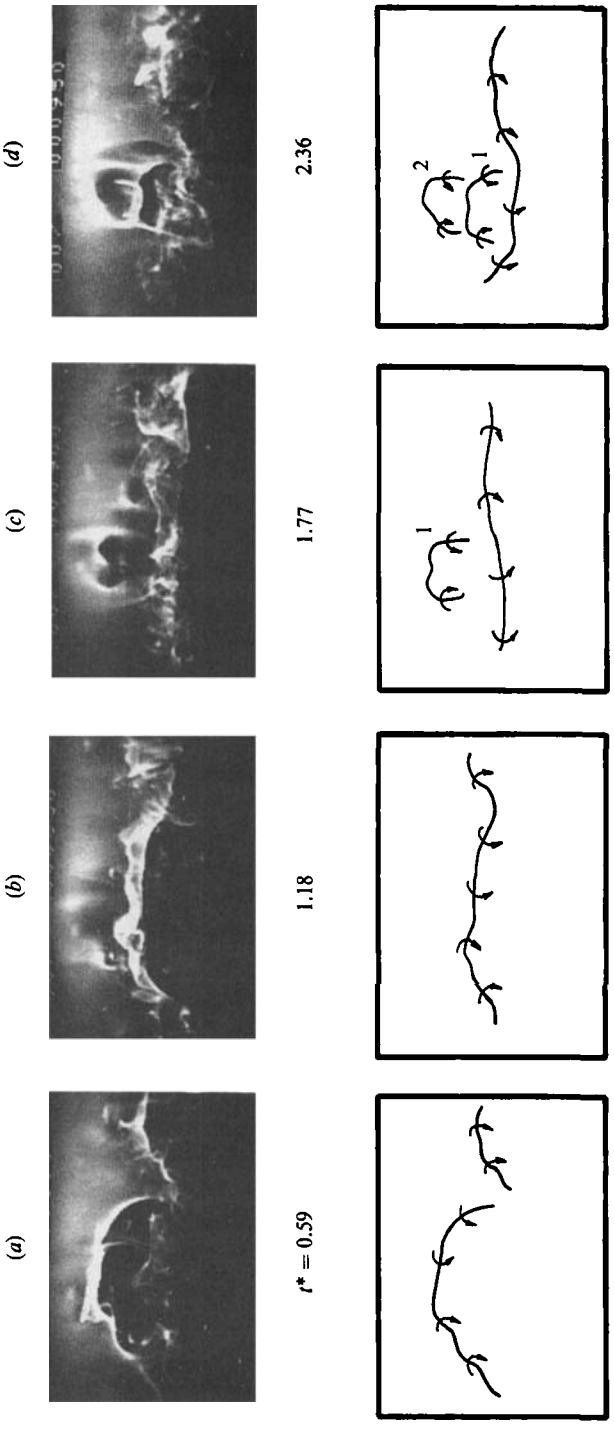

FIGURE 9. Top-view sequence showing the cellular deformation of the secondary vortices shed from a 4.83 cm cylinder at $Re_d = 3570$. $t^* = \Delta t U_\infty / d$. Note the lack of cellular development relative to figures 5 and 8.

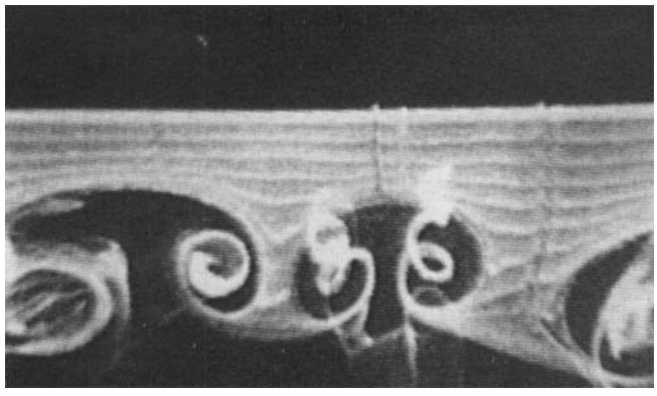

FIGURE 10. Top-view photograph of axial vortex pairs behind a 1.27 cm cylinder at $Re_d \approx 1000$.

result in smaller spanwise cells with correspondingly narrower spacing. The present results are consistent with these suggested modes of variation.

Section A–A in figure 7 demonstrates the mushroom-type pattern that streamwise stretched secondary vortices will yield when viewed in cross-section. A photograph showing the coherence of these axial vortex pairs as they appear in the near wake of a 1.27 cm diameter cylinder at a Reynolds number of approximately 1000 is shown in figure 10. Note that the pattern suggested by section A–A in figure 7 and demonstrated in figure 10 is strikingly similar to both the cross-stream visualization pictures of Bernal (1981), Lasheras *et al.* (1986), and the isovorticity contours of the mixing-layer 'braids' of Lin (1981).

Figure 10 is also clearly suggestive of how the formation and deformation of the secondary vortices contribute to the turbulent mixing process. That counter-rotating vortex pairs can be visually observed indicates that periodic spanwise mixing is taking place across the shear layer; unmarked fluid is passing through the bubble sheet and creating the mushroom shapes identified as vortex pairs. Because the secondary vortices lie in the separated boundary layer, they both entrain high-speed fluid down into the formation region and eject low-speed fluid up into the free stream. It is hypothesized that this mixing process plays a key role in the transition from vortex streets to turbulent wakes.

3.2. *Relation between f_1/f_v and Re_d*

The first task of the quantitative study was to establish the dependence of the non-dimensional secondary-vortex shedding frequency f_1/f_v on Reynolds number Re_d, where f_1 is the secondary-vortex-shedding frequency, f_v is the Strouhal-vortex shedding frequency and Re_d is the Reynolds number based on cylinder diameter. Bloor (1964) introduced this form of non-dimensional frequency as a direct result of a dimensional argument relating the secondary-vortex-shedding frequency to the Strouhal number, the free-stream velocity, and the separated cylinder boundary-layer thickness. While the validity of Bloor's argument is addressed in §4, the secondary-vortex shedding frequency will be non-dimensionalized and plotted against Reynolds number in the fashion consistent with that initiated by Bloor.

Figure 11 is a log–log plot of the results determined from visualization studies of the 2.54 cm, 3.81 cm and 4.83 cm cylinders. The error bars represent one standard deviation about the mean of the measurements taken for each point. It can be

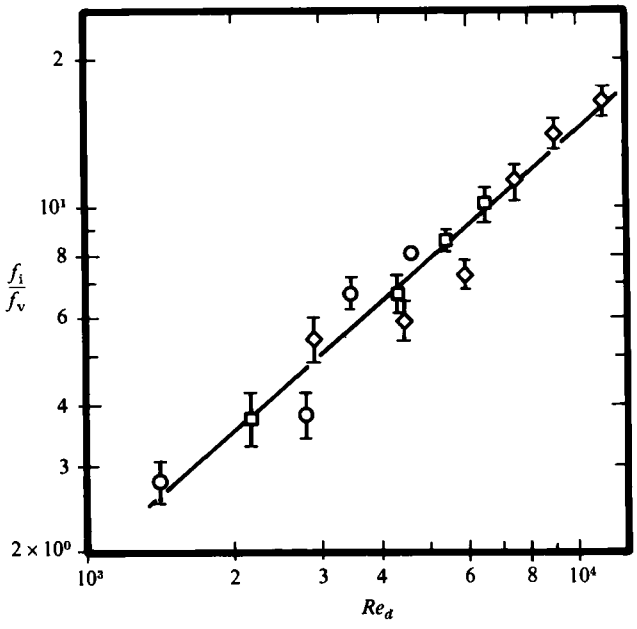

FIGURE 11. Plot of the non-dimensional shedding frequency versus Reynolds number obtained from visualization studies of the smallest three cylinders. The equation of the representative line is $f_i/f_v = (Re_d/470)^{0.87}$. ○, $d = 2.54$ cm; □, 3.81 cm; ◇, 4.83 cm.

observed that the data lies approximately on a straight line, suggesting that a power-law relation exists between the shedding frequency and Reynolds number.

Thus, each set of data in figure 11 were fitted to a power-law curve using regression techniques. The resulting equations were determined to be

$$f_i/f_v = (Re_d/489)^{0.904} \quad \text{for } d = 2.54 \text{ cm},$$

$$f_i/f_v = (Re_d/507)^{0.907} \quad \text{for } d = 3.81 \text{ cm},$$

$$f_i/f_v = (Re_d/532)^{0.907} \quad \text{for } d = 4.83 \text{ cm}.$$

A test for similarity of these three regression curves, the test for the equality of two lines outlined by Neter & Wasserman (1974), suggests that within 90 % accuracy the regression lines are statistically indistinguishable. The apparent similarity between data sets suggested the validity of a power-law-curve fit of the cumulative data, which yields the general relation

$$f_i/f_v = (Re_d/470)^{0.87},$$

with a coefficient of correlation of $r = 0.974$.

The positive slope of the data in figure 11 supports the speculation that secondary vortices contribute to the transition of vortex streets. As the Reynolds number approaches 10^5, the limit where the cylinder boundary layer becomes turbulent and the vortex street disappears, it is expected that the secondary vortices will be the dominant structure in the cylinder near wake. Bloor (1964) reported that the point at which transition from laminar Strouhal vortices to turbulent Strouhal vortices occurs will move continually closer to the cylinder with increasing Reynolds number. She also determined that transition waves are detected in essentially the same streamwise location where the Strouhal vortices undergo transition from laminar to turbulent behaviour.

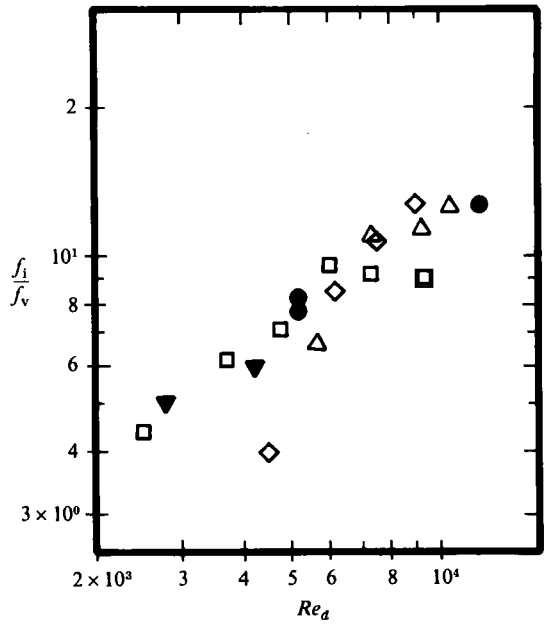

FIGURE 12. Plot of the frequency data obtained from spectral analysis of hot-wire-anemometry measurements for the largest three cylinders: □, $d = 3.81$ cm; ◇, 4.83 cm; △, 5.84 cm. Bloor's 0.63 cm (▼) and 2.54 cm (●) cylinder data are included for comparison.

3.3. *Anemometry study*

An attempt was made to reproduce the power-law relation for secondary vortex shedding using a hot-wire anemometer as a detection device. The anemometer probe was placed at a non-dimensional location $x/d = 0.6$ and $y/d = 0.6$, consistent with the previous experimental study of Bloor (1964). The anemometer signal was filtered and then input into the MINC-11 mini-computer. Data were obtained using a FORTRAN program which performed a fast Fourier transform of the data yielding power spectra of the filtered anemometer signals.

The non-dimensional secondary-vortex shedding-frequency data are shown in figure 12, plotted in log–log form as a function of Reynolds number. Comparable data from Bloor (1964) are also plotted, and indicate a marked similarity to the present results. In order to compare this similarity of the two data-acquisition methods employed in the present study, the regression line of the lumped (i.e. combined 3.81 cm, 4.83 cm and 5.84 cm data) anemometry data, and the regression line for the flow-visualization data are shown in figure 13. The equations of the respective lines are

$$f_i/f_v = (Re_d/410)^{0.773}$$

for the lumped anemometry data, and

$$f_i/f_v = (Re_d/470)^{0.87}$$

for the lumped flow-visualization data. Although quite similar, the anemometry results appear to yield generally lower values of f_i/f_v at comparable Reynolds numbers. This is thought to be due to a certain amount of information loss in the measurement and processing of the anemometer data, as explained below.

The primary difficulty with using anemometry to detect the secondary-vortex shedding behaviour is that one is attempting to detect a developing, Lagrangian

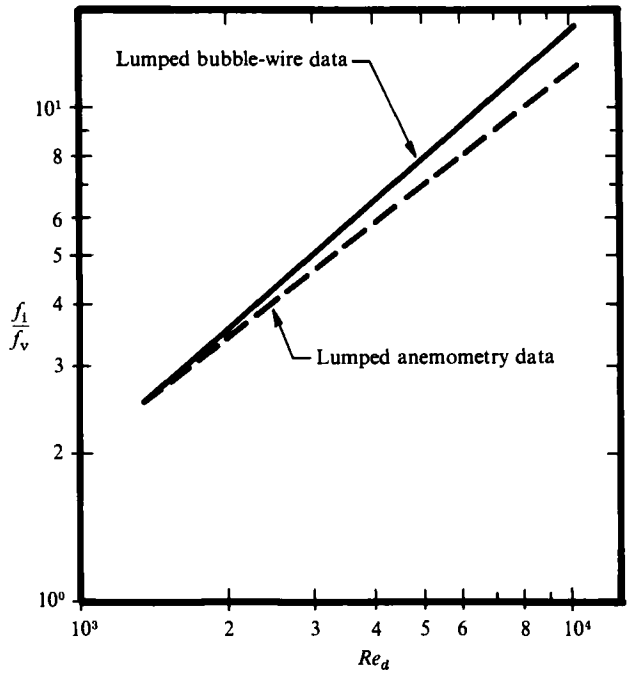

FIGURE 13. Comparison of the regression line of the combined (i.e. lumped) anemometry data (dotted line) and the representative line of the flow-visualization data (solid line). The equations of the two lines are: $f_l/f_v = (Re_d/409)^{0.773}$ and $f_l/f_v = (Re_d/470)^{0.87}$, for the anemometry and the visualization data respectively.

phenomenon with a stationary, Eulerian probe. At a given streamwise location, the separated cylinder boundary layer oscillates in the vertical direction as a direct consequence of the formation of the Strouhal vortices. Thus the hot-wire probe, placed as it was at a non-dimensional location of $x/d = 0.6$ and $y/d = 0.6$, will only sense secondary instabilities during the times when the separated boundary layer is in proximity to the probe. This results in an anemometer signal which reveals the characteristic frequency of the secondary vortices only intermittently. The intermittency of the signal, when transformed into the frequency domain, gives rise to spurious peaks in the power spectrum which are not characteristic of the secondary vortices. Filtering of the signal to delete the effects of the intermittency and the Strouhal-vortex shedding frequency, and thus isolate the secondary-vortex shedding frequency, proved quite difficult, particularly for cases where all three frequencies were of the same order of magnitude. This ultimately led to a limitation in the confidence of the anemometry results. However, within the limits of experimental accuracy, the anemometry data appear to indicate a clear correlation between the Bloor transition waves and the secondary-vortex phenomenon. This is further supported by the lack of visual evidence of any additional phenomena in the near-wake region which demonstrate frequency characteristics similar to those of the secondary vortices.

4. General discussion and comments

The hypothesized model of secondary-vortex development is consistent with previous observations of three-dimensional structures in the near wake of cylinders. The cellular deformation of the vortices was shown to result in the development of

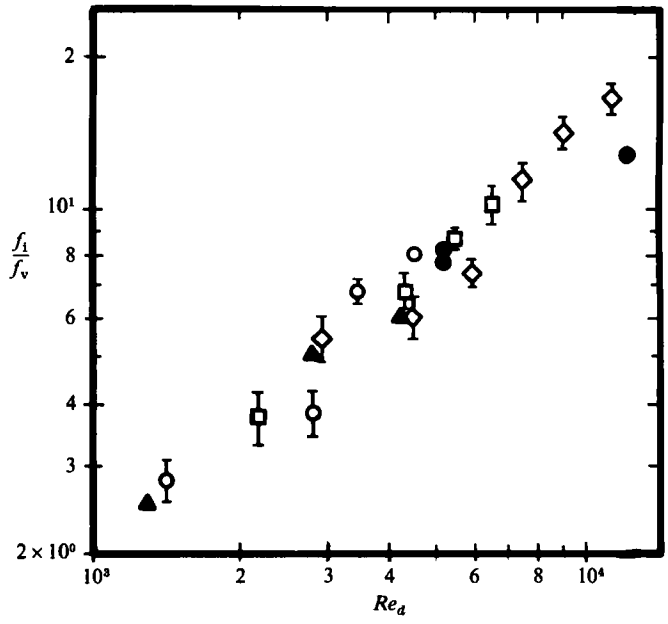

FIGURE 14. Plot of the non-dimensional shedding frequency versus Reynolds number for the smallest three cylinders: ○, $d = 2.54$ cm; □, 3.81 cm; ◇, 4.83 cm. Bloor's 0.63 cm (▲) and 2.54 cm (●) cylinder data are included for comparison.

'axial vortex pairs', which are subsequently stretched by the action of the Strouhal vortices to form 'fingers'. The 'knots' described by Gerrard (1978) are probably a manifestation of these 'axial vortices', but his dye-visualization technique did not allow him to observe the rotational motion of the structures. The similarities between the secondary-vortex development, free-shear-layer transition, and Tollmien–Schlichting waves beg speculation of the existence of a universal transition mechanism. Bloor (1964) was leading to such a speculation when she hypothesized that her 'transition waves' were Tollmien–Schlichting waves generated in the separated boundary layer.

The apparent positive correlation between Bloor's transition-wave data and similar data taken for the secondary vortices is shown in figure 14. Although the two data sets appear essentially identical, it should be noted that a rigorous statistical correlation between the two data sets cannot be demonstrated. This is because (i) Bloor presented very little data in this Reynolds-number range, and (ii) her measurements may have been subject to the same limitations described in §3.4. However, within the limits of the present investigation there appears to be a clear correlation between transition waves and secondary vortices.

Bloor (1964) reported that f_i/f_v appeared to scale as the 0.5 power of Re_d, which she argued was consistent with dimensional considerations. However, the present results suggest an approximately 0.87 power-law scaling, almost twice that proposed by Bloor. To address this discrepancy between Bloor's results and those of the present study, Bloor's dimensional arguments are outlined and evaluated below.

Bloor first assumed that f_v scaled on U_∞/d and that f_i should scale on U_∞/δ, where δ is the boundary-layer thickness on the cylinder. She then assumed a boundary-layer relationship of $\delta/d \propto U_\infty^{-\frac{1}{2}}$, as suggested by Schlichting (1979), to obtain a scaling of $f_i/f_v \propto Re_d^{\frac{1}{2}}$. Bloor cites her 2.54 cm cylinder data to support this relationship.

However, there are two serious limitations to her analysis. The first is the

assumption that f_i should scale on boundary-layer thickness, rather than on a characteristic thickness more reflective of the separated shear layer. As pointed out in §1.2 of this paper, it appears to be more reasonable to assume that secondary vortices are generated as a consequence of a free-shear instability which keys on a momentum thickness characteristic of the middle of the linear growth region of the separated boundary layer. The second limitation is that Bloor supports her analysis with only three data points, two of which were taken at the same Reynolds number. Interestingly, if one fits a regression line to all of Bloor's data, it yields a proportionality of $f_i/f_v \propto Re_d^{0.73}$. This power relation is almost identical to that obtained in the present study using hot-wire anemometry. It also corresponds more closely to the 0.87 power determined from the visualization data than to the 0.5 power predicted by Bloor's analysis.

The rationale for the 0.87 power Reynolds-number dependence of f_i/f_v seems to lie in the fact that the instability frequency appears to have its origin as a free-shear instability, and is characterized by a momentum thickness reflective of the linear growth region. The location of this characteristic momentum thickness depends on Reynolds number and cylinder diameter; it should move towards the separation point with increasing Reynolds number. This was shown by Bloor (1964) and more recently by Unal & Rockwell (1986).

Extrapolation of the 0.87 power relation to low Reynolds numbers indicates that the secondary and Strouhal shedding frequencies should become equal for Reynolds numbers in the range where Strouhal vortices first demonstrate turbulent characteristics (approximately 300–400). This again invites speculation that it may be the onset of the secondary-vortex behaviour which initiates the transition from laminar to turbulent Strouhal vortices.

5. Conclusions

Secondary vortices generated in the near wake of circular cylinders were examined using two independent measurement techniques: hydrogen-bubble flow visualization and hot-wire anemometry. The results of a systematic evaluation of these measurements lead to the following conclusions:

secondary vortices and transition waves, previously observed by Bloor, appear to be identical phenomena;

the non-dimensional shedding frequency of the secondary vortices is roughly proportional to the 0.87 power of Reynolds number, contrary to the 0.5 power law reported by Bloor;

the secondary vortices appear to result from a free-shear instability in the near wake which causes the separated cylinder boundary layer to roll up;

rapid distortion of the secondary vortices into cellular structures in the near wake appears to result in a strong spanwise mixing which may be the mechanism of transition from laminar to turbulent Strouhal vortices.

We wish to thank Dr D. O. Rockwell for reviewing the original manuscript and providing several helpful suggestions for improvement. In addition, we would like to acknowledge partial support of this work under a grant from the Air Force Office of Scientific Research.

REFERENCES

BEARMAN, P. W. 1965 Investigation of the flow behind a two-dimensional model with a blunt trailing edge and fitted with splitter plates. *J. Fluid Mech.* **21**, 241–255.

BERNAL, L. P. 1981 The coherent structure of turbulent mixing layers. I. Similarity of the primary vortex structure. II. Secondary streamwise vortex structure. Ph.D. thesis, California Institute of Technology, Pasadena.

BLOOR, M. S. 1964 The transition to turbulence in the wake of a circular cylinder. *J. Fluid Mech.* **19**, 290–304.

BREIDENTHAL, R. 1979 Chemically reacting, turbulent shear layer. *AIAA J.* **17**, 310–311.

BROWAND, F. K. 1965 An experimental investigation of the instability of an incompressible, separated shear layer. *MIT Rep.* ASRL TR92-4.

CAIN, A. B., REYNOLDS, W. C. & FERZINGER, J. H. 1981 A three-dimensional simulation of transition and early time decaying mixing layer. *Stanford University Rep. No.* TF-14.

FREYMUTH, P. 1966 On transition in a separated laminar boundary layer. *J. Fluid Mech.* **25**, 683–704.

GERRARD, J. H. 1978 The wakes of cylindrical bluff bodies at low Reynolds number. *Phil. Trans. R. Soc. Lond.* A **288**, 351–382.

HAMA, F. R. 1963 Progressive deformation of a perturbed line vortex filament. *Phys. Fluids* **6**, 526–534.

HO, C. M. & HUANG, L. S. 1982 Subharmonics and vortex merging in mixing layers. *J. Fluid Mech.* **119**, 443–472.

HO, C. M. & HUERRE, P. 1984 Perturbed free-shear layers. *Ann. Rev. Fluid Mech.* **16**, 365–424.

HO, C. M. & NOSSEIR, N. S. 1981 Dynamics of an impinging jet. Part I. The feedback phenomenon. *J. Fluid Mech.* **105**, 119–42.

KONRAD, J. H. 1976 An experimental investigation of mixing in two-dimensional turbulent shear flows with applications to diffusion-limited chemical reactions. *Project SQUID Tech. Rep.* CIT-8-PU.

LASHERAS, J. C., CHO, J. S. & MAXWORTHY, T. 1986 On the origin and evolution of streamwise vortical structures in a plane, free shear layer. *J. Fluid Mech.* (in press).

LIN, S. J. 1981 The evolution of streamwise vorticity in the free shear layer, Ph.D. thesis, University of California, Berkeley.

MICHALKE, A. 1965 On spatially growing disturbances in an inviscid shear layer. *J. Fluid Mech.* **23**, 521–544.

MICHALKE, A. 1969 A note on spatially growing three-dimensional disturbances in a free shear layer. *J. Fluid Mech.* **38**, 765–767.

MICHALKE, A. & HERMANN, G. 1982 On the inviscid instability of a circular jet with external flow. *J. Fluid Mech.* **114**, 343–359.

NETER, J. & WASSERMAN, W. 1974 *Applied Linear Statistical Models.* Richard D. Irwin, Inc.

SCHLICHTING, H. 1979 *Boundary Layer Theory*, 7th edn, pp. 215–216. McGraw-Hill.

SMITH, C. R. & METZLER, S. P. 1983 The characteristics of low-speed streaks in the near-wall region of a turbulent boundary layer. *J. Fluid Mech.* **129**, 27–54.

UNAL, M. F. & ROCKWELL, D. O. 1986 On vortex formation from a cylinder. Part I. The initial instability. *J. Fluid Mech.* (to appear).

WEI, T. & SMITH, C. R. 1980 The appearance of axial vortices in vortex shedding from a cylinder. *Bull. Am. Phys. Soc.* **25**, 1092.